Dyslipidemia at the crossroad of the skin barrier and the arterial wall

Martins Cardoso, R.

Chapter 5

Barrier lipid composition and response to plasma lipids: a direct comparison of mouse dorsal back and ear skin

Experimental Dermatology 29(6): 548-555 (2020).

Renata Martins Cardoso[1], Samira Absalah[1], Miranda Van Eck[1*], Joke A. Bouwstra[*]

[1]Division of BioTherapeutics, Leiden Academic Centre for Drug Research, Leiden University, Leiden, The Netherlands

*Both authors contributed equally

ABSTRACT

The skin of the ear and the back are frequently selected sites in skin research using mouse models. However, distinct responses to treatment have been described between these two sites in several studies. Despite the crucial role of the stratum corneum (SC) in the skin barrier function of both dorsal back and ear skin, it remains unclear whether differences in lipid composition might underlie altered responses. Here, we compared the skin morphology and the barrier lipid composition of the ear with the back skin of wild-type mice. The ear contained more corneocyte layers in the SC and its barrier lipid composition was enriched with sphingosine ceramide subclasses, especially the short ones with a total chain length of 33-34 carbon atoms. The free fatty acid (FFA) profile in the ear skin shifted towards shorter chains, significantly reducing the mean chain length to 23.3 versus 24.7 carbon atoms in the back skin. In line, FFA species in the ear displayed a 2-fold increase in unsaturation index ($p<0.001$). Gene expression in the ear skin revealed low expression of genes involved in lipid synthesis and uptake, indicating a reduced metabolic activity. Finally, the effects of hypercholesterolemia on the SC FFA composition of the ear and the back skin was assessed in apolipoprotein E knockout (*APOE*$^{-/-}$) mice. Interestingly, the FFA profile in *APOE*$^{-/-}$ ear skin was minimally affected, while the FFA composition in the *APOE*$^{-/-}$ back skin was markedly changed in response to hypercholesterolemia. In conclusion, ear and back skin have distinct barrier lipids and respond differently to elevated plasma cholesterol.

Keywords: *Ceramides, fatty acids, wild-type mice, apolipoprotein E knockout mice*

1. INTRODUCTION

Our understanding of skin morphology and lipid composition has benefitted greatly from the use of *in vivo* animal models[1–3]. In particular, mouse models have been proven a valuable tool in skin research as it offers the possibility to genetically manipulate these animals to study the role of specific skin components (*e.g.* enzymes, proteins, receptors) and to generate *in vivo* diseased skin models[1,2]. In research, the back skin and the ear skin of mice are commonly used sites. However, previous studies reported differential effects/phenotypes on ear skin versus the back skin regarding, among others, drug treatment (*e.g.* imiquimod-induced psoriasis, allergic contact dermatitis), melanocyte function, and tissue regeneration[4–6]. The back skin comprises a relatively large area for performing experiments, but in hairy mice it contains a high density of hair follicles (fur) that can complicate the interpretation of the results[5]. In most studies, the fur is shaved to allow skin treatment and analysis. At the same time, the hair follicles may offer an alternative pathway for compound permeation[7,8]. In contrast, the ear represents an easily accessible, but small, skin area with a low density of hair follicles and centrally supported by a cartilaginous tissue framework[5].

Regardless of the skin site, the stratum corneum (SC) has a critical role in skin barrier function protecting against body desiccation and harmful chemicals and pathogens[9]. The SC is a well-organized structure of corneocytes (dead cornified keratinocytes) surrounded by an extracellular lipid matrix with free fatty acids (FFAs), ceramides (CERs), and cholesterol as major lipid classes[10]. Currently, however, there are no studies comparing SC lipids as the primary barrier components in the back versus ear skin. The lipids constituting the SC matrix are mostly synthesized by differentiating keratinocytes[10] or taken up from the plasma via lipoprotein receptors (*e.g.* low-density lipoprotein receptor, scavenger receptor class B member I (SR-BI), and cluster of differentiation 36 (CD36))[11–13]. For the skin barrier function the only continuous pathway connecting the environment with the viable epidermis is the SC extracellular lipid matrix[14]. Alterations in the composition of these lipids have been described in various skin pathologies, and it has been demonstrated that the SC lipids are crucial for the primary barrier components in the skin[15–20]. Exogenous molecules can penetrate the skin via this SC lipid matrix, particularly when the SC lipid profile is modified in response to (environmental) stressors and inflammatory processes.

Recently, we showed that increased plasma lipoprotein levels as described for apolipoprotein E knockout (*APOE*$^{-/-}$) and *SR-BI*$^{-/-}$ mice are associated with an altered lipid profile in the back skin at young age, affecting mainly the FFA composition[21,22]. In the severely hypercholesterolemic *APOE*$^{-/-}$ mice these epidermal lipids changes led

to functional differences in transepidermal water loss towards a less effective skin barrier. *APOE*$^{-/-}$ mice and other hypercholesterolemic mouse models have recently been used to study the relation between psoriasis and the comorbidities dyslipidemia and atherosclerosis[23–25]. Differential effects in *APOE*$^{-/-}$ mice have been described in response to the induction of psoriasis-like skin inflammation by topical application of compounds on ear *vs* back skin, with the back skin being more effective in generating the desired phenotype[6,26]. As lipids play a major role in the skin barrier, it is crucial to understand whether the epidermal lipid barrier in the ear is similarly impacted by hypercholesterolemia as previously demonstrated for the back skin of *APOE*$^{-/-}$ mice.

In this study, we used young adult wild-type (WT) mice to compare the morphology, lipid composition and gene expression between dorsal and ear skin. In addition, the epidermal lipid composition of the well-established hypercholesterolemic *APOE*$^{-/-}$ mice was also analyzed to assess whether the ear skin develops similar differences in lipid matrix composition in response to hypercholesterolemia as previously described for the back skin of these mice[22].

2. MATERIALS AND METHODS

2.1 Materials and chemicals

Rodent chow diet low in fat and cholesterol (Rat and Mouse No.3 breeding diet) purchased from Special Diets Services (United Kingdom). We obtained ketamine and atropine from AUV Veterinary Services (Cuijk, The Netherlands) and xylazine from ASTFarma (Oudewater, The Netherlands). Sodium phosphate dibasic (Na_2HPO_4), hematoxylin, eosin, trypsin from bovine pancreas, trypsin inhibitor, free fatty acids with 16 to 30 carbon atoms (FFA C16-30), deuterated FFA C18, deuterated FFA C24, chloroform, safranin-O, acetic acid, trifluoroacetic acid were obtained from Sigma-Aldrich (Zwijndrecht, The Netherlands). Heptane was purchased from ChemLab (Zedelgem, Belgium). Tissue-Tek O.C.T. was purchased from Sakura Finetek Europe B.V. (The Netherlands). Sodium chloride (NaCl) was purchased from Boom (Meppel, The Netherlands). Synthetic CER CER[N(C24deuterated)S(C18protonated)] were kindly provided by Evonik Industries (Essen, Germany). From Merck (Darmstadt, Germany) we bought potassium dihydrogen phosphate (KH_2PO_4), potassium chloride (KCl), potassium hydroxide and Entellan®. Methanol, ethanol, isopropanol and acetonitrile were from Biosolve (Valkenswaard, The Netherlands). All solvents had analytical grade.

2.2 Animals and samples

16-18 weeks old female C57BL/6 WT mice and female *APOE*$^{-/-}$ mice (obtained from The Jackson Laboratory and bred at the Gorlaeus laboratories) were kept under standard laboratory conditions (20°C and light cycle of 12 hours light/12 hours dark) with water and standard low-fat chow diet provided ad libitum (Rat and Mouse No.3 breeding diet). Prior sacrifice, the mice were anesthetized with a mixture of xylazine, atropine and ketamine (70 mg/kg; 1.8 mg/kg; 350 mg/kg body weight, respectively) and perfused with phosphate buffered saline (PBS; 8.13 g/L NaCl, 2.87 g/L Na_2HPO_4, 0.2 g/L KH_2PO_4, 0.19 g/L KCl in milliQ water; pH 7.4). The ears (WT and *APOE*$^{-/-}$ mice) and the shaved back skin (WT mice) were processed for morphological stainings (hematoxylin and eosin, and safranin-O), epidermal lipid composition analysis (liquid chromatography/mass spectrometry; LC/MS) and gene expression analysis (q-PCR). For sebum lipids analysis, hairs were collected from the back skin of both WT and *APOE*$^{-/-}$ mice. The sebum lipid composition was analyzed by LC/MS. Experiments were performed in agreement with National guidelines and approved Animal Experiments Ethics Committee of Leiden University.

2.3 Morphology stainings

Both ear and dorsal skin were embedded in tissue-tek and snap-frozen in liquid nitrogen. Frozen sample sections (8 µm) were rinsed in PBS and stained with hematoxylin and eosin according to manufacturer's protocol. The sections were mounted in DPX and imaged with a Zeiss Axioplan 2 light microscope (Zeiss, Best, The Netherlands). Frozen skin sections (8 µm) were fixed in cold acetone for 10 min and incubated with safranin-O solution (1% safranin-O in milliQ water) for 1 min. The sections were rinsed in milliQ to remove the excess of safranin-O and incubated with KOH solution (2% KOH in milliQ water) for 20 minutes[27]. The slides were covered with coverslip and imaged with a Zeiss Axioplan 2 light microscope (Zeiss, Best, The Netherlands).

2.4 Epidermal lipid extraction

The epidermis was isolated from the dorsal skin by trypsinization (0.3 % w/v trypsin in PBS; pH 7.4). Skin samples without the hypodermis were stretched on a paper filter soaked in 0.3 % w/v trypsin solution in PBS (pH 7.4) overnight at low temperature (4°C) for trypsin diffusion throughout the samples. Next day, the dorsal skin was incubated at 37°C (1 hour) for trypsin activation and subsequent isolation of the epidermis. Afterwards, the trypsin in the samples was neutralized by washing the samples in 0.1% w/v trypsin inhibitor in PBS and in demi-water. After air-drying, the samples were

placed under argon atmosphere for storage and further SC lipid extraction. The ears were used directly for lipid extraction as epidermal separation by trypsinization was not possible. Instead, a piece of the ear was completely submerged in the solvent mixes for lipid extraction. Considering that murine skin has few corneocytes layers and a thin epidermis compared to human skin, also for the ear likely the barrier lipids from the epidermis were extracted. Hairs were removed from the back skin using tweezers and used to extract sebum lipids. Epidermal lipids from the ear and the back and the sebum lipids surrounding the hairs were extracted with a modified Bligh and Dyer method described previously[28]. Lipid extracts in chloroform:methanol (2:1; v/v) and under argon atmosphere were kept at 4°C for liquid chromatography-mass spectrometry (LC/MS) CER and FFA analysis.

2.5 Liquid chromatography-mass spectrometry (LC/MS)

LC/MS analysis of epidermal and sebum CERs and FFAs was performed as described previously[22]. For CER analysis, 5 µL of lipid extracts reconstituted in heptane:chloroform:methanol (95:2.5:2.5; v/v/v) at a lipid concentration of 0.3 mg/mL were injected in an Acquity UPLC H-class system (Waters, Milford, MA, USA) connected to a triple-quadrupole XEVO TQ-S mass spectrometer (Waters, Milford, MA, USA). A normal phase column (PVA-Sil column: 5 µm particle size, 100x2.1 mm i.d., YMC, Kyoto, Japan) was used for CER separation with the solvent flow rate set to 0.8 ml/min (Supplementary Table S1). The MS was coupled to atmospheric pressure chemical ionization (APCI) chamber set to positive ion mode and the detector measured in full scans from 350-1200 amu. Software Waters MassLynx 4.1 was used to determine the area under the curve (AUC) followed by internal standard correction for CER analysis. Deuterated CER NS (C24 deuterated; C18 protonated) was used as internal standard. CERs were further analyzed according to a method described by Boiten *et. al.* (2016)[28]. CER data was plotted as relative molar percentage of ceramide subclasses based on the total amount of CERs. CER subclasses in this paper were identified using the nomenclature described by Motta *et. al.* (1993)[29]. For FFA analysis, 2 µl of lipid extracts reconstituted in isopropanol to a lipid concentration of 0.75 mg/mL were injected in the same UPLC-mass spectrometry system described for the CERs. As internal standards, deuterated FFA C18 and FFA C24 were added to all samples prior their injection into the UPLC-system. FFAs were separated in the UPLC system using a Purospher Star LiChroCART reverse phase column (3 µm particle size, 55x2 mm i.d., 55x2 mm, Merck, Darmstadt, Germany) with the solvent flow rate set to 0.5 mL/min (Supplementary Table S2). The XEVO TQ-S mass spectrometer connected to an APCI chamber (probe temperature: 425°C, discharge current 3 µA.) was set to negative mode and detector measured in full scan from 200-550 amu. FFA Data analysis was performed by Software

Waters MassLynx 4.1 to determine the AUC followed by internal standard correction. Response was calculated based on calibration curves of FFA C16-C30. Data was presented as relative molar percentage to the total amount of FFA detected. Saturated and unsaturated FFA C16-C18 are highly present in sebum lipids and were plotted separately (data not shown).

2.6 qPCR

Total RNA was isolated from ear and dorsal skin samples (without hypodermis) by the guanidinium thiocyanate method[30]. cDNA was synthetized from 1 µg total RNA (M-MuLV reverse transcriptase, ThermoFisher Technologies). Quantitative analysis of the genes (QuantStudio 6 Flex Real-time PCR systems, Applied Biosystems, Foster City, CA, USA) was done using SYBR Green detection technology. The expression of the target genes was normalized by the expression of the reference genes beta-actin (*β-actin*) and fatty acid binding protein 5 (*FABP5*). The expression of target genes in the ear and dorsal skin was plotted as relative fold change compared to the gene expression in the dorsal skin. Information regarding the forward and reverse primer sequences is available in Supplementary Table S3.

2.7 Statistical analysis

Data is presented as mean±SD and statistical significance was calculated using GraphPad Prism 8 (GraphPad Software Inc., CA, USA). *P* values below 0.05 were considered significant.

3. RESULTS

3.1 Thicker SC layer in the ear skin compared to the back skin

The general morphology of the ear skin and back skin of wild-type C57BL/6 mice was assessed by hematoxylin and eosin (HE), and safranin-O stainings (Fig. 1). HE staining of the ear showed a central cartilaginous structure. The hypodermis was more pronounced in the back skin than in ear skin. The dermis and epidermis presented comparable morphology between the two different skin sites. Safranin-O staining revealed a higher number of corneocyte layers in the ear SC compared to the back skin. In the latter, corneocytes showed more expansion in response to the alkali environment during the safranin-O staining

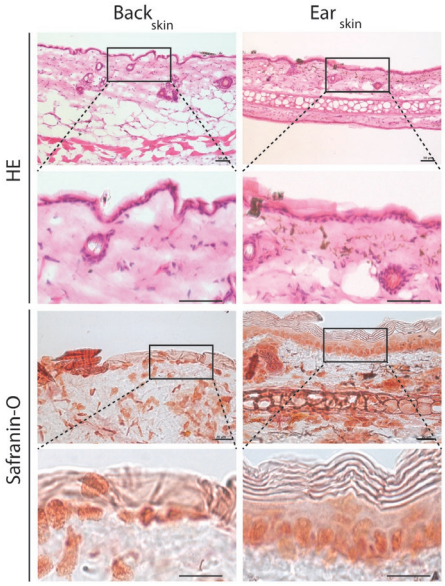

Figure 1. Epidermal and dermal morphology of back skin and ear skin. Back skin and ear cryostat sections (8 µm) stained with (a) hematoxylin and eosin (HE, scale bar: 50 µm) and (b) safranin-O (scale bar: 20 µm). Micrographs representative of 3 WT mice.

3.2 Epidermal CER composition strongly differs between dorsal and ear skin

For epidermal CER analysis, the epidermis was isolated from dermis in the back skin and used for lipid extraction (Fig. 2a). For the ear skin, lipids were extracted from the most distal section of the ear (Fig. 2b). Subsequently, the composition of CERs in the extracted lipids was analyzed by LC/MS. CER subclasses nomenclature is a combined representation of the acyl chains (non-hydroxy fatty acid [N]; α-hydroxy fatty acid [A] or esterified ω-hydroxy fatty acid [EO]) with the sphingoid base (dihydrosphingosine, [dS]; sphingosine [S] or phytosphingosine [P]) as reported by Motta *et. al.* (1993)[29]. The molar percentage distribution of the CER subclasses was strikingly different in the ear skin compared with the back skin (Fig 2c). The majority of the CERs are sphingosine base (CER[S]) at both skin sites (55% in the back skin vs 75% in the ear skin). Nonetheless, in the back skin CER NdS is most abundantly present (nearly 40%), while in ear skin NS and AS are present at higher concentrations (45% and 28%, respectively) than in back skin. The ω-esterified CERs (CER[EO]), composed of CER EOS and EOdS, represented 7% of the CERs in the back skin. In the ear skin CER EOS accounted for 14% of the CER content whereas CER EOdS was not detected. The CER[non-EO] chain length

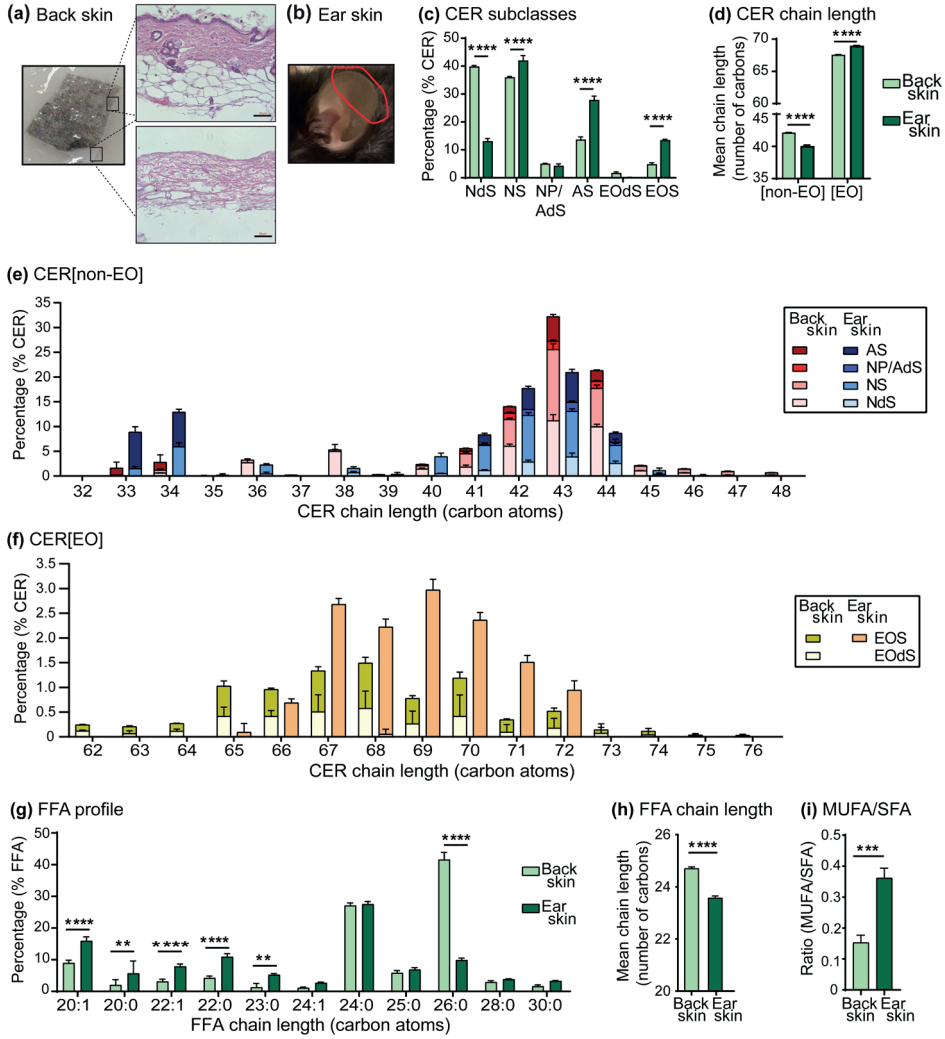

Figure 2. CER and FFA composition of the ear and back skin. CERs and FFAs were quantified by LC/MS. Representative images showing (a) epidermis isolation from back skin and (b) distal part of the ear (red circled area) used for lipid extraction. CERs are named according to nomenclature described by Motta *et. al.* (1993); (c) Distribution of CER subclasses (% molar); (d) CER mean chain length; total CER chain length distribution (e) CER[nonEO] and (f) CER[EO]; (g) FFA chain length distribution (molar %); (h) mean FFA chain length; (i) molar ratio between monounsaturated FAs (MUFA) and saturated FAs (SFA). Statistical significance was determined by Two-way ANOVA with Holm-Sĭdak post-hoc test and by two-tailed unpaired Student's T-test. Data presented as mean±SD (molar); n=3-4 samples/group; **p<0.01; ***p<0.001; ****p<0.0001.

distribution revealed higher abundance of long chain CERs (≥43 carbon atoms) in the back skin, while ear skin showed increased presence of short chain length CERs

(≤42 carbon atoms). Among the short chain CERs, the C33 and C34 CERs were strongly present in ear skin (22%) compared to back skin (5%) (Fig. 2d-e). The mean chain length of CER[non-EO] was shorter in the ear (39.5 carbon atoms vs. 41.8 carbon atoms in the back skin). When focusing on CER [EO], in the back skin, the mean chain length was 67.7 carbons while in the ear skin this average was 68.9 carbons (p<0.0001) with marked detection of CERs with 62-65 carbons, which were merely present in the ear skin (Fig. 2d-f).

3.3 Skin lipids in the ear are enriched in short and unsaturated FFA species

The composition of the FFAs with a chain length between 20-30 carbons atoms in the ear and the back skin was determined by LC/MS. The FFA composition of the ear skin showed a shift towards shorter and more unsaturated FFA species (Fig. 2g). In the back skin, FFA C24:0 and FFA C26:0 were most prevalent FFAs, accounting for nearly 70% of the total amount of FFAs (Fig. 2g). In the ear skin, FFA C20:1 and C24:0 were most abundant, comprising 43% of the FFAs with a striking four-fold reduction in the percentage of FFA C26:0 to only 10% (Fig. 2g). These differences strongly contributed to a shorter mean FFA chain length of 23.3 carbons in the ear compared to an average FFA chain length of 24.5 carbons atoms in the back skin (p<0.0001) (Fig. 2h). The mol ratio between mono-unsaturated FAs (MUFAs) and saturated FAs (SFAs) was 2-fold higher in the ear FFA species (0.36±0.03) than in the back FFAs (0.15±0.02) (p<0.001) (Fig. 2i).

3.4 Lower basal mRNA levels of genes involved lipid synthesis in the ear skin

The expression of genes involved in lipid synthesis and keratinocyte proliferation and differentiation was assessed to determine the underlying factors responsible for the differences in lipid composition in the ear and in the back skin. Basal mRNA levels of genes involved in cholesterol synthesis (*HMGCS1*; 2-fold), esterification (*ACAT1*; 3-4-fold) and uptake of lipoproteins (*LDLR*; 2-fold) were significantly lower in the ear compared to the back skin (Fig. 3a). In addition, the ear also showed a nearly 70% reduction in the expression *CERS3* and *GBA* (synthesis of esterified-ω-CERs and cleavage of glucosyl-CERs, respectively) with no changes in the expression of *DEGS1* (enzyme involved in synthesis step of CER[S] from CER[dS]) (Fig. 3b). Expression of fatty acid synthase (*FAS*) was reduced by 30% in the ear while expression of *SCD1*, an enzyme involved in fatty acid chain desaturation, was comparable between groups (Fig. 3c). The ear also showed reduced expression of genes involved in FFA chain elongation; *ELOVL1* (2-fold) and *ELOVL4* (3-fold) (Fig. 3c). In line with the lower expression of genes related to lipid synthesis, mRNA levels of *DGAT2* (triglyceride synthesis) and *ABCA12* (lipid transport to lamellar bodies) were also decreased in

the ear skin (Fig. 3d). The back skin showed higher expression of genes involved in keratinocyte differentiation (*IVL*) and proliferation (*K10*) markers (p<0.0001) (Fig. 3d).

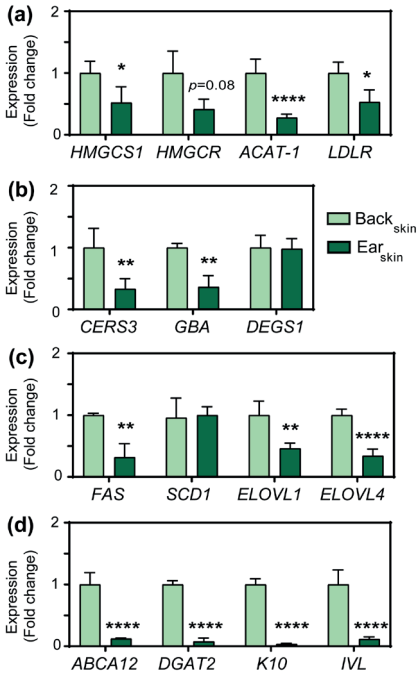

Figure 3. Ear skin shows lower expression levels of several genes involved in skin lipid metabolism and keratinocyte markers. mRNA levels of genes related to the synthesis or uptake of (a) cholesterol; synthesis of (b) CERs; and (c) FFAs. Expression of genes linked to (d) lipid transport in lamellar bodies; triglyceride (TG) synthesis; and keratinocyte proliferation and differentiation. Statistical significance was determined by two-tailed unpaired Student's T-test; *p<0.05; **p<0.01; ****p<0.0001. Data presented as mean±SD; n=5/group.

3.5 Changes in plasma lipid composition differentially affect dorsal and ear skin

The back skin of hypercholesterolemic *APOE*$^{-/-}$ mice shows an altered FFA profile in response to the massively increased levels of apolipoprotein B containing lipoprotein particles in the circulation at young age[22]. It remains unknown whether the skin in the ears is similarly affected by this hypercholesterolemic profile. Thus, next, we analyzed the FFA composition in the ear of *APOE*$^{-/-}$ mice and compared it to that described for WT ear skin in Figure 2g. The relative distribution of FFA (% total FFA) in the ear of *APOE*$^{-/-}$ mice was nearly comparable to the composition described for WT ear (Fig. 4a). The FFA composition in the ear of *APOE*$^{-/-}$ mice showed a significant increase in the percentage of FFA C20:0 (p<0.0001) accompanied by reduction in the percentage of FFA C24:0

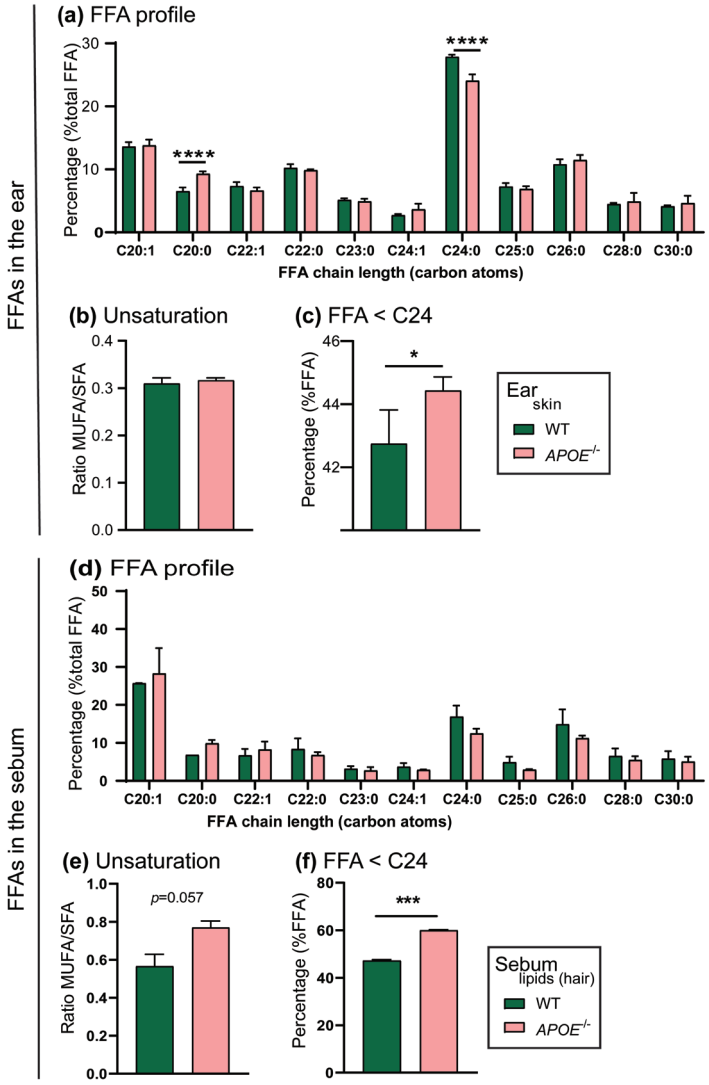

Figure 4. FFA composition of the ear and of sebum in normolipidemic WT and hypercholesterolemic *APOE*$^{-/-}$ mice. FFA profile: (a) FFA chain length distribution profile in the ear skin; (b) molar ratio between monounsaturated FFAs (MUFA) and saturated FFAs (SFA) in the ear skin; (c) percentage of short chain FFA (FFA chains containing less than 24 carbon atoms) in the ear skin; (d) FFA chain length distribution profile in the sebum lipids; (e) molar ratio between monounsaturated FFAs (MUFA) and saturated FFAs (SFA) in the sebum lipids; (f) percentage of short chain FFA (FFA chains containing less than 24 carbon atoms) in the sebum lipids. Statistical significance was determined by One-way ANOVA with Holm-Sĭdak post-hoc test and by two-tailed unpaired Student's T-test. Data presented as mean±SD; n=3-4 samples/group; *p<0.05; ****p<0.0001.

(p<0.0001). Consequently, a small shift towards a shorter chain length was observed in the ear of *APOE*$^{-/-}$ mice (Fig. 4b). The molar ratio between monounsaturated and saturated FFA species was not altered (Fig. 4c). Sebum lipids, produced by sebaceous glands, contribute to the skin surface lipid pool, particularly in back skin with a high density of hair follicles, and hence, sebaceous glands[31]. Triglycerides, a component of sebum lipids, may undergo hydrolysis by microbial lipases generating FFAs[32–34]. Thus, next we compared the composition of the FFAs in the sebum surrounding back skin hairs of both WT and *APOE*$^{-/-}$ mice to assess whether the sebum of *APOE*$^{-/-}$ mice was affected by the hypercholesterolemic profile of these mice. The sebum FFA composition of WT and *APOE*$^{-/-}$ mice was overall comparable (Fig. 4d), indicating that the observed differential response to hypercholesterolemia between back and ear skin cannot be explained by effects on the FFA content of sebum.

4. DISCUSSION

In mouse models both ear and back skin have been proven valuable assets in a large range of skin studies[1–3]. However, similarities and differences between ear and back skin are not extensively examined. In the present study, we provide evidence that the lipid composition of the skin barrier is fundamentally different between the two sites, as is the expression of genes related to lipid synthesis and keratinocytes differentiation and proliferation. In addition, the skin of the ear showed only a minimal response to hypercholesterolemic conditions as compared to the back skin.

The density of hair follicles and the number of corneocyte layers in the SC are important factors in skin research as they directly relate to skin permeability and, thus, barrier function. In hairy mice, the high density of hair follicles provides a smaller interfollicular area and comprises a permeation pathway into the skin. In the hairy C57Bl6 mouse strain, melanin production is restricted to the hair follicles and absent in the skin. Melanin is mostly produced during the anagen phase of the hair growth, giving the skin a dark pigmentation[35]. As hair growth in the murine skin occurs in waves, it leads to the formation of dark pigmented areas (dark patches) and non-pigmented areas ("white" patches). The dark skin patches with synchronized hair cycles appear after the age of 10 weeks[35]. In this study, "white" skin patches at similar position in the back skin were used for analysis as different hair cycles can influence the skin response to compounds and even the development of inflammation[25,36]. The SC in these "white" back skin patches of hairy mice has fewer number of corneocyte layers as compared to ear skin. The back skin of nude-mice with a larger interfollicular area displays a thicker SC with more corneocyte layers[37], suggesting that the reduced number of corneocyte layers in hairy mice is a direct effect of the presence of dense hair follicles and/or fur.

The reduced number of corneocyte layers in the back skin may require a faster turnover/replacement to preserve the barrier, whilst in the ear skin this turnover may take longer. Also, the ear skin has a lower density of blood vessels as well as lymphatic vessels than the back skin indicating a reduced metabolic activity and even drainage in the ear[6,38,39]. Accordingly, the basal expression of genes related to lipid synthesis/uptake and keratinocyte differentiation and proliferation was significantly higher in the back skin, likely reflecting the more active metabolic profile at this site.

The mRNA expression of the enzymes *CERS3, ELOVL1,* and *ELOVL4* was lower in ear skin as compared to back skin. *CERS3* encodes for the main ceramide synthase involved in the synthesis of CER[EO] and it regulates the elongation of FA chains by ELOVL1 and ELOVL4[40]. *In vitro* co-expression of *CERS3* with *ELOVL1* leads to an augmented production of CERs with a C26:0 acyl chain which is also accompanied by an increase in CERs with a C24:0 acyl chain[40]. Further elongation of C26:0 FAs is continued by ELOVL4 to generate both CER[non-EO] and CER[EO] with acyl chains containing more than 26 carbon atoms[40]. *In vivo*, *ELOVL1*$^{-/-}$ mice and *ELOVL4*$^{-/-}$ mice show a remarkable reduction in CER[EO] content and a shift towards CER containing acyl chains shorter than 24 carbons atoms[40,41]. Despite the low levels of *CERS3* in the ear skin, CER[EO] accounted for a relatively high percentage of the CERs in the ear skin, which may be a result of the overall percentage distribution of each subclass. Surprisingly, the mean chain length of CER[EO] was higher in the ear skin where reduced expressions of *ELOVL1* and *ELOVL4* were observed. Remarkably, the skin of *ELOVL4*$^{-/-}$ mice also showed major increases in the prevalence of CER NS and CER AS, especially containing acyl chain C26:0[42]. In the present study, the ear skin showed high prevalence of CER[S], while the expression of *DEGS1*, encoding for the desaturase enzyme that converts CER[dS] into CER[S][43], was comparable to the back skin, indicating that the reduced expression of *ELOVL4* can be related to the accumulation of CER NS and CER AS[42]. In line, the reduced expression of *CERS3, ELOVL1* and *ELOVL4* in the ear skin resulted in an increase in the fraction of sphingosine CERs with a total chain length of 33 and 34 carbon atoms, especially in CER NS and CER AS subclasses. Although CERs are essential components of the skin barrier, little information is available regarding the mechanism(s) involved in the regulation of ceramide synthesis[44]. Other factors, not included in the scope of this study (*e.g.* acyl-coenzyme A-binding protein), may also impact CER synthesis and contribute to the results described here[44].

The changes in the FFA composition in the ear corroborate with the reduced expression of *ELOVL1* and *ELOVL4* in the ear skin, leading to a FFA profile enriched with shorter chains. The ear skin also showed a higher presence of unsaturated FFA species compared to the back skin, although no changes were observed in the basal expression of *SCD1*,

an enzyme tightly regulated and subjected to fast turn on/off expression[45,46]. Altogether, our LC/MS and PCR data show that the skin lipid composition largely varies with the anatomical site even within young adult WT mice. Elucidation of the underlying causes for the reported differences between ear and back skin warrants further investigation.

As lipids are important components of the SC, variations in the skin lipid composition can affect the barrier function. In atopic dermatitis patients, the CER profile shows increased levels of CER NS and CER AS and a reduction of the average chain length linked to increased levels of C34 CERs in these subclasses[47]. These patients also have a higher percentage of short and unsaturated FFA species in their skin lipids[47]. Human skin equivalents, bioengineered *in vitro* models of human skin often containing activated keratinocytes, also show similar changes in lipid profile[48]. In both atopic dermatitis skin and in human skin equivalents samples, the altered lipid composition results in a reduced barrier function of the skin compared to native human skin[47,48]. In this view, it is likely that the changes in lipid composition described here for the ear skin is not favorable for an optimal lipid barrier, which may lead to higher number of corneocyte layers in order to compensate for this unfavorable lipid profile.

Lipids provided by plasma lipoproteins are also incorporated into the skin and hence an imbalance in lipoprotein profile may affect the composition of the barrier lipid pool[21,22,38,49]. Hypercholesterolemic *APOE*$^{-/-}$ mice develop skin inflammation and lipid deposits in the dermal compartment upon aging and when fed a high cholesterol/high fat diet[50,51]. Remarkably, already at young age, the back skin of these hypercholesterolemic mice shows altered epidermal lipid composition prior to the development of inflammatory skin profiles[22]. The FFA composition is especially affected in the back skin showing enrichment in short and unsaturated chains. In contrast, in the current study we found that the ear skin of young *APOE*$^{-/-}$ mice is minimally affected with only a minor shift towards shorter FFA chains. Considering the faster turnover of corneocyte layers in the back skin in combination with higher density of lymphatic and blood vessels, this skin site can more readily reflect the changes in the plasma lipids. Our findings provide insight why, as previously described, the ear and the back skin react differently to specific treatments leading to distinct outcomes; *e.g.* imiquimod-induced psoriasis[6].

In conclusion, the morphology and lipid composition of murine skin significantly varies depending on the body location, specifically in the ear and in the back skin. We suggest that the turnover rate of the corneocyte layer in combination with the level of metabolic activity of the skin site can be key players in the response to therapeutic intervention and to systemic lipid changes. Nonetheless, defining which skin site should be used in studies is not straightforward as the skin is a complex organ. It is important to further

characterize the morphological-, inflammatory-, and metabolic variations amongst skin sites in order to better match the skin site to the goal of the study.

CONFLICT OF INTEREST

The authors have declared no conflict of interest.

ACKNOWLEDGEMENTS

This research was funded by the Leiden Academic Centre for Drug Research (Leiden, The Netherlands).

REFERENCES

1. Avci, P. et al. Animal models of skin disease for drug discovery. Expert Opin. Drug Discov. 8, 331–355 (2013).

2. Abd, E. et al. Skin models for the testing of transdermal drugs. Clin. Pharmacol. Adv. Appl. Volume 8, 163–176 (2016).

3. Todo, H. Transdermal permeation of drugs in various animal species. Pharmaceutics 9, 1–11 (2017).

4. Nguyen, T. & Wei, M. L. Hermansky–Pudlak HPS1/pale ear Gene Regulates Epidermal and Dermal Melanocyte Development. J. Invest. Dermatol. 127, 421–428 (2007).

5. Metcalfe, A. D., Willis, H., Beare, A. & Ferguson, M. W. J. Characterizing regeneration in the vertebrate ear. J. Anat. 209, 439–446 (2006).

6. Madsen, M., Pedersen, T. X., Nielsen, L. B., Johansen, C. & Hansen, P. R. Differential Effects of Digoxin on Imiquimod-Induced Psoriasis-Like Skin Inflammation on the Ear and Back. Ann. Dermatol. 30, 485 (2018).

7. Mohd, F., Todo, H., Yoshimoto, M., Yusuf, E. & Sugibayashi, K. Contribution of the hair follicular pathway to total skin permeation of topically applied and exposed chemicals. Pharmaceutics 8, (2016).

8. Blume-Peytavi, U. et al. Follicular and percutaneous penetration pathways of topically applied minoxidil foam. Eur. J. Pharm. Biopharm. 76, 450–453 (2010).

9. Elias, P. M. Stratum corneum defensive functions: An integrated view. J. Invest. Dermatol. 125, 183–200 (2005).

10. Ponec, M., Weerheim, A., Lankhorst, P. & Wertz, P. New acylceramide in native and reconstructed epidermis. J. Invest. Dermatol. 120, 581–588 (2003).

11. Lin, M.-H. & Khnykin, D. Fatty acid transporters in skin development, function and disease. Biochim. Biophys. Acta 1841, 362–8 (2014).

12. Mommaas, M., Tada, J. & Ponec, M. Distribution of low-density lipoprotein receptors and apolipoprotein B on normal and on reconstructed human epidermis. J. Dermatol. Sci. 2, 97–105 (1991).

13. Tsuruoka, H. et al. Scavenger receptor class B type I is expressed in cultured keratinocytes and epidermis. Regulation in response to changes in cholesterol homeostasis and barrier requirements. J. Biol. Chem. 277, 2916–2922 (2002).

14. Sahle, F. F., Gebre-Mariam, T., Dobner, B., Wohlrab, J. & Neubert, R. H. H. Skin Diseases Associated with the Depletion of Stratum Corneum Lipids and Stratum Corneum Lipid Substitution Therapy. Skin Pharmacol. Physiol. 28, 42–55 (2015).

15. Zheng, Y. et al. PEG-Based Hydrogel Synthesis via the Photodimerization of Anthracene Groups. Macromolecules 35, 5228–5234 (2002).

16. Zhang, X. et al. Piezofluorochromic properties and mechanism of an aggregation-induced emission enhancement compound containing N-hexyl-phenothiazine and anthracene moieties. J. Phys. Chem. B 115, 7606–11 (2011).

17. Zhang, X.-X. et al. pH-Sensitive Fluorescent Dyes: Are They Really pH-Sensitive in Cells? Mol. Pharm. (2013). doi:10.1021/mp3006903

18. Janssens, M. et al. Increase in short-chain ceramides correlates with an altered lipid organization and decreased barrier function in atopic eczema patients. J. Lipid Res. 53, 2755–2766 (2012).

19. Hoekstra, M. et al. Absence of HDL cholesteryl ester uptake in mice via SR-BI impairs an adequate adrenal glucocorticoid-mediated stress response to fasting. J. Lipid Res. 49, 738–745 (2008).

20. van Smeden, J. et al. Intercellular Skin Barrier Lipid Composition and Organization in Netherton Syndrome Patients. J. Invest. Dermatol. 134, 1238–1245 (2014).

21. Martins Cardoso, R. et al. Hyperalphalipoproteinemic scavenger receptor BI knockout mice exhibit a disrupted epidermal lipid barrier. Biochim. Biophys. Acta - Mol. Cell Biol. Lipids 1865, 158592 (2020).

22. Martins Cardoso, R. et al. Hypercholesterolemia in young adult APOE −/− mice alters epidermal lipid composition and impairs barrier function. Biochim. Biophys. Acta - Mol. Cell Biol. Lipids 1864, 976–984 (2019).

23. Madsen, M. et al. Imiquimod-Induced Psoriasis-Like Skin Lesions Do Not Accelerate Atherosclerosis in Low-Density Lipoprotein Receptor–Deficient Mice. Am. J. Pathol. 188, 1486–1496 (2018).

24. Xie, X. et al. Imiquimod induced ApoE-deficient mice might be a composite animal model for the study of psoriasis and dyslipideamia comorbidity. J. Dermatol. Sci. 88, 20–28 (2017).

25. Madsen, M. et al. Effect of 12-O-tetradecanoylphorbol-13-acetate-induced psoriasis-like skin lesions on systemic inflammation and atherosclerosis in hypercholesterolaemic apolipoprotein E deficient mice. BMC Dermatol. 16, 9 (2016).

26. Schaper, K. et al. Sphingosine-1-phosphate exhibits anti-proliferative and anti-inflammatory effects in mouse models of psoriasis. J. Dermatol. Sci. 71, 29–36 (2013).

27. Oudshoorn, M. H. M. et al. Development of a murine model to evaluate the effect of vernix caseosa on skin barrier recovery. Exp. Dermatol. 18, 178–184 (2009).

28. Boiten, W., Absalah, S., Vreeken, R., Bouwstra, J. & van Smeden, J. Quantitative analysis of ceramides using a novel lipidomics approach with three dimensional response modelling. Biochim. Biophys. Acta - Mol. Cell Biol. Lipids 1861, 1652–1661 (2016).

29. Motta, S. et al. Ceramide composition of the psoriatic scale. BBA - Mol. Basis Dis. 1182, 147–151 (1993).

30. Chomczynski, P. & Sacchi, N. The single-step method of RNA isolation by acid guanidinium thiocyanate–phenol–chloroform extraction: twenty-something years on. Nat. Protoc. 1, 581–585 (2006).

31. Pappas, A., Johnsen, S., Liu, J.-C. & Eisinger, M. Sebum analysis of individuals with and without acne. Dermatoendocrinol. 1, 157–161 (2009).

32. Maier, H. et al. Normal Fur Development and Sebum Production Depends on Fatty Acid 2-Hydroxylase Expression in Sebaceous Glands. J. Biol. Chem. 286, 25922–25934 (2011).

33. Feldman, A. et al. Blimp1+ cells generate functional mouse sebaceous gland organoids in vitro. Nat. Commun. 10, 2348 (2019).

34. Dahlhoff, M. et al. Sebaceous lipids are essential for water repulsion, protection against UVB-induced apoptosis and ocular integrity in mice. Development 143, 1823–1831 (2016).

35. Plikus, M. V. & Chuong, C.-M. Complex Hair Cycle Domain Patterns and Regenerative Hair Waves in Living Rodents. J. Invest. Dermatol. 128, 1071–1080 (2008).

36. Hofmann, U., Tokura, Y., Nishijima, T., Takigawa, M. & Paus, R. Hair Cycle-Dependent Changes in Skin Immune Functions: Anagen-Associated Depression of Sensitization for Contact Hypersensitivity in Mice. J. Invest. Dermatol. 106, 598–604 (1996).

37. Rissmann, R., Oudshoorn, M. H. M., Hennink, W. E., Ponec, M. & Bouwstra, J. A. Skin barrier disruption by acetone: observations in a hairless mouse skin model. Arch. Dermatol. Res. 301, 609–613 (2009).

38. Liu, F., Smith, J., Zhang, Z., Cole, R. & Herron, B. J. Genetic heterogeneity of skin microvasculature.

Dev. Biol. 340, 480–489 (2010).

39. Huggenberger, R. et al. An important role of lymphatic vessel activation in limiting acute inflammation. Blood 117, 4667–4678 (2011).

40. Sassa, T. et al. Impaired Epidermal Permeability Barrier in Mice Lacking Elovl1, the Gene Responsible for Very-Long-Chain Fatty Acid Production. Mol. Cell. Biol. 33, 2787–2796 (2013).

41. Khnykin, D., Miner, J. H. & Jahnsen, F. Role of fatty acid transporters in epidermis: Implications for health and disease. Dermatoendocrinol. 3, 53–61 (2011).

42. Li, W. et al. Depletion of ceramides with very long chain fatty acids causes defective skin permeability barrier function, and neonatal lethality in ELOVL4 deficient mice. Int. J. Biol. Sci. 120–128 (2007). doi:10.7150/ijbs.3.120

43. Ternes, P., Franke, S., Zähringer, U., Sperling, P. & Heinz, E. Identification and Characterization of a Sphingolipid Δ4-Desaturase Family. J. Biol. Chem. 277, 25512–25518 (2002).

44. Ferreira, N. S. et al. Regulation of very-long acyl chain ceramide synthesis by acyl-CoA-binding protein. J. Biol. Chem. 292, 7588–7597 (2017).

45. Sampath, H. & Ntambi, J. M. Role of stearoyl-CoA desaturase-1 in skin integrity and whole body energy balance. J. Biol. Chem. 289, 2482–2488 (2014).

46. Mauvoisin, D. & Mounier, C. Hormonal and nutritional regulation of SCD1 gene expression. Biochimie 93, 78–86 (2011).

47. van Smeden, J. et al. The importance of free fatty acid chain length for the skin barrier function in atopic eczema patients. Exp. Dermatol. 23, 45–52 (2014).

48. Helder, R. W. J. et al. The effects of LXR agonist T0901317 and LXR antagonist GSK2033 on morphogenesis and lipid properties in full thickness skin models. Biochim. Biophys. Acta - Mol. Cell Biol. Lipids 1865, 158546 (2020).

49. Huang, L. et al. Interleukin-17 Drives Interstitial Entrapment of Tissue Lipoproteins in Experimental Psoriasis. Cell Metab. 29, 475-487.e7 (2019).

50. Feingold, K. R. et al. Apolipoprotein E Deficiency Leads to Cutaneous Foam Cell Formation in Mice. J. Invest. Dermatol. 104, 246–250 (1995).

51. Ang, L. S., Cruz, R. P., Hendel, A. & Granville, D. J. Apolipoprotein E, an important player in longevity and age-related diseases. Exp. Gerontol. 43, 615–622 (2008).

SUPPLEMENTARY INFORMATION

1. METHODS

1.1 Liquid chromatography-mass spectrometry (LC/MS)

Table S1. Gradient of solvents used for cholesterol and CER analysis by UPLC-LC/MS.

Run time (min)	Solvent A[1] (%)	Solvent B[2] (%)
0	98	2
2.5	96	4
2.6	93	7
6	88	12
11	50	50
13	98	2

[1]Solvent A - 100% Heptane

[2]Solvent B -Heptane:isopropanol:ethanol - 50:25:25; v/v/v

Table S2. Gradient of the solvents used for FFA analysis by UPLC-LC/MS.

Run time (min)	Solvent A[1] (%)	Solvent B[2] (%)
0	100	0
2.5	0	100
5	0	100
8	100	0
11	100	0

[1]Solvent A - Acetonitrile/milliQ/chloroform/acetic acid -90:10:2:0.005; v/v/v/v

[2]Solvent B -Methanol/heptane/chloroform/acetic acid -90:10:2:0.005; v/v/v/v

Table S3. Forward and reverse primer sequences used for q-PCR.

Protein (Gene)	Forward primer Reverse primer
Beta-actin (βACTIN)	CTTCTTTGCAGCTCCTTCGTTGCCG AATACAGCCCGGGGAGCATCGTC
Fatty acid binding protein 5 (FABP5)	GGACGGGAAGGAGAGCACGATAACA GCACCTTCTCATAGACCCGAGTGCA
ATP-binding cassette, subfamily A, member 12 (ABCA12)	GGAAGATGGCGTCCGCTCTGTG GTGAGATGTGCTGGGTCATGTGGAC
Acetyl-Coenzyme A acetyltransferase 1 (ACAT1)	AGCTGTTTCTCTGGGCCATCCAAT GAACTCTCCTGGCTTCAGGGCAT
Ceramide synthase 3 (CERS3)	GGGCCTCCACGTTTACTGGGGT GCCCTTGGTGCTCTCTGCTTCCT
Delta(4)-desaturase, sphingolipid 1 (DEGS1)	GAGCACCATGACTTCCCCAACGTTC CAGGAGTTGTAGTGCGGGAGGTCAT
Diacylglycerol O-acyltransferase 2 (DGAT2)	TATTGGTTTCGCCCCCTGCATCTTC ATGTCTTTCTGGGTCGGGTGCTC
Elongation of very long chain fatty acids 1 (ELOVL1)	GGCAGAACTTGCCCCTGAGAAGAA TTCACAACAGCCTCCATCCTGGC
Elongation of very long chain fatty acids 4 (ELOVL4)	TGGAATCAAGTGGGTGGCTGGAGG AGCATGGTCAGGTATCGCTTCCACC
Fatty acid synthase (FAS)	GGCGGCACCTATGGCGAGG CTCCAGCAGTGTGCGGTGGTC
Glucocerebrosidase (GBA)	GCCCTTGCCAACAGTTCCCATGATG TGCCATGAACGTACTTAGCTGCCTCT
3-hydroxy-3-methylglutaryl-CoA reductase (HMGCR)	CGAGCCACGACCTAATGAAGAATG TGCATCACTAAGGAACTTTGCACC
3-hydroxy-3-methylglutaryl-CoA synthase 1 (HMGCS1)	AAAACACAGAAGGACTTACGCCCGG GTTGCAGGGAGTCTTGGCACTTTCT
Involucrin (IVL)	CCTCTGCCTTCTCCCTCCTGTGAGT ACACAGTCTTGAGAGGTCCCTGAACCA
Keratin 10 (K10)	GCGGCGACCAATCATCTAAAGGACC CCAGTGGCCCGTATGAAGAGACTCT
Low density lipoprotein receptor (LDLR)	TGTGTGATGGAGACCGAGATTG CGTCAACACAGTCGACATCC
Stearoyl-Coenzyme A desaturase 1 (SCD1)	TACTACAAGCCCGGCCTCC CAGCAGTACCAGGGCACCA